

Dispersions of multi-wall carbon nanotubes in ferroelectric liquid crystals

M. Yakemseva¹, I. Dierking^{2,a}, N. Kapernaum³, N. Usoltseva¹, and F. Giesselmann³

¹ Ivanovo State University, Nanomaterials Research Institute, Ermak str. 39, 153025, Ivanovo, Russia

² School of Physics and Astronomy, University of Manchester, Oxford Road, Manchester, M13 9PL, UK

³ Institute of Physical Chemistry, University of Stuttgart, Pfaffenwaldring 55, 70569 Stuttgart, Germany

Received 29 October 2013 and Received in final form 25 January 2014

Published online: 18 February 2014 – © EDP Sciences / Società Italiana di Fisica / Springer-Verlag 2014

Abstract. The electro-optic and dielectric properties of ferroelectric liquid crystal–multi-wall carbon nanotube dispersions were investigated with respect to temperature and nanotube concentration. The main physical properties, such as tilt angle, spontaneous polarization, response time, viscosity, and Goldstone-mode relaxation strength and frequency were studied. While all dispersions exhibit the expected temperature dependencies of their physical properties, their dependence on nanotube concentration is still a controversial discussion in literature, with several contradicting reports. For increasing nanotube concentration we observed a decrease in tilt angle, but an increase in spontaneous polarisation, the latter explaining the enhancement of the bilinear coupling coefficient, and the dielectric relaxation strength. Despite the increase in polarization, the electro-optic response times slow down, which suggests an increase of rotational viscosity along the tilt cone. It is anticipated that the latter also accounts for the observed decrease of the Goldstone-mode relaxation frequency for increasing nanotube concentration.

1 Introduction

Dispersions of carbon nanotubes with liquid crystals have attracted much interest in recent years, due to the possibility to produce and design new materials with added functionality. Nanotubes [1] have extraordinary properties, which are related to their strong shape anisotropy, such as a large electric conductivity anisotropy, being large along their long axis, while being much lower across it. Similarly, they exhibit a large elastic modulus along the long axis, while at the same time being flexible. Respective anisotropies can also be observed for other physical properties, for example heat conductivity. Liquid crystals (LCs) [2,3] are mainly known for their applications in flat panel displays, optical shutters or light modulators, but more areas of applications are currently evolving, for example in the fields of photonics or sensors. LCs are anisotropic fluids, thermodynamically located between the isotropic liquid and the three dimensionally ordered crystal. They are self-organized systems with only partial order, which can be orientational order along the average long axis of the elongated molecules, called the director \mathbf{n} (nematic phase), or additional one- or two-dimensional positional order, which represents the smectic phases. Based on symmetry considerations, Meyer *et al.* [4] concluded that every tilted smectic phase which is formed by chi-

ral molecules exhibits a spontaneous polarization. If this polarization can be reoriented between two stable states we speak of ferroelectricity and ferroelectric liquid crystals (FLC) [5]. This behavior is realized in the surface stabilized geometry (SSFLC), introduced by Clark and Lagerwall [6], where the intrinsic helical superstructure of the SmC* phase is unwound by the surface interactions between the liquid crystal and the confining substrates.

The fundamental idea of liquid crystal-nanotube dispersions is the transfer of self-organized order of the liquid crystal onto the dispersed nanotubes, which can be of the single-wall or the multi-wall type, through elastic interactions of the nanotubes with the liquid crystal director field [7,8]. Most investigations to date have been carried out on thermotropic nematic liquid crystals with positive or negative dielectric anisotropy, but reports can also be found for thermotropic discotic phases [9–11] and lyotropic liquid crystals [12–16], while nanotubes themselves can form lyotropic liquid crystalline phases at high concentrations [17,18]. A very useful review of liquid crystal-nanotube dispersions can be found by Lagerwall and Scalia [19]. In addition to the orienting effect of the liquid crystal, the selected orientation direction of the nanotubes can dynamically be changed, due to a range of different switching mechanisms of various liquid crystal phases, such as the electric [20,21] and magnetic [22] Freedericksz effect, ferroelectric switching, or the electroclinic effect.

^a e-mail: ingo.dierking@manchester.ac.uk

Only few reports have been published which investigate FLC-nanotube dispersions [23–30], involving both single-wall and multi-wall tubes. Most of the studies were concerned with the dielectric properties of these hybrid systems and individual electro-optic parameters. Several of these investigations led to controversial results, exhibiting behavior of opposite trends.

In this paper we systematically investigate the effect of carbon nanotubes on ferroelectric liquid crystals, specifically the SmC* phase, as a function of carbon nanotube concentration and temperature. The phase diagram is presented, and detailed results of all important material parameters, tilt angle θ , spontaneous polarization P_S , bilinear polarization-tilt coupling, response time τ , rotational viscosity γ , dielectric strength and Goldstone-mode relaxation frequency of the FLC-nanotube dispersions are discussed.

2 Experiment

The ferroelectric liquid crystal mixture Felix M4851/050 (Clariant, Germany, with a phase sequence of *Cryst.* -15°C SmC* 67.7°C SmA* 72.7°C N* 79.1°C *Iso.*) was chosen as the liquid crystal host material. The multi-wall carbon nanotubes (MWCNTs) were provided by Taunit-M, Nanotechcenter, Russia, and were used as received. They were produced by chemical vapor deposition using a Ni/Mg catalyst. Carbon nanotube characterization was carried out by Raman spectroscopy before sonification (Horiba Jobin Yvon LabRam HR800 spectrometer equipped with a He-Ne laser ($\lambda = 633\text{ nm}$) operating at 20 mW) and atomic force microscopy (Veeco Nanoscope Dimension 3100 AFM operating in the tapping mode with Si cantilever).

The FLC-MWCNTs dispersions were prepared using a solvent dispersion method. Firstly, the dispersion of 0.1 mg CNTs in 1 ml of dichloromethane was obtained by ultra sound sonication for 20 minutes using a UIS 250 V sonotrode from Dr. Hielscher GmbH working at 24 kHz and 250 W. Then, small quantities of this dispersion were added to the respective liquid crystal and sonicated again for 30 min. The residual solvent was subsequently removed by evaporation. The weight concentration of MWCNTs was varied between 0.005 and 0.04 wt%. Aggregation of the nanotubes during the isotropic to liquid crystal phase transition cannot be excluded, as this is a common effect due to van der Waals interactions. Nevertheless, this was not obvious from polarization microscopy.

Samples were introduced into commercial sandwich cells (AWAT, Poland) of thickness $5\ \mu\text{m}$ by capillary action. Cells had indium tin oxide (ITO) electrodes with an active area of $5.0 \times 5.0\ \text{mm}^2$ and antiparallel rubbed polyimide alignment layers for planar orientation of the liquid crystal.

Phase transition temperatures of all FLC-MWCNT dispersions were determined using a Leica DMLP polarizing microscope combined with an Instec TS62 hot stage and an Instec SCT 200 temperature controller for

relative temperature accuracy of 0.1 K. Electro-optic parameters of the respective materials depending on temperature and nanotube concentration, were measured using an experimental setup consisting of a He-Ne laser (Laser 2000 LHRP-0501, $\lambda = 633\text{ nm}$), linear polarizer, quarter-wave plate, and a rotating analyzer. Electric fields were applied by a function generator (Kontron Electronic pulse 8021) in combination with a high voltage amplifier (Krohn-Hite 7500). Electro-optic responses were monitored via a low-noise preamplifier (Stanford Research System SR 560) and an oscilloscope (Tektronix TDS 460A). Temperatures were controlled by a Julabo F25HP controller to within 0.5 K. The spontaneous polarization P_S was determined by the well-known triangular wave method [31]. Measurements were carried out in the SmC* temperature range at an applied field amplitude of $1.07\ \text{V}/\mu\text{m}$ and frequency 70 Hz.

The temperature dependence of the electro-optic switching times of the FLC-MWCNTs dispersions was obtained by employing a standard polarizing microscope based electro-optic set up consisting of a Leica DMLP microscope with a fast photo diode (FLC Electronics, Sweden), an oscilloscope (Tektronix TDS 460A), a function generator (TOELLNER TOE 7704) and a voltage amplifier (FLC Electronics, Sweden). Rise times were defined as the change in transmission between 10% to 90% of the optic response to the applied square wave voltage of above stated amplitude and frequency.

The dielectric behavior of all samples was investigated by means of dielectric spectroscopy in the frequency range from 5 Hz to 13 MHz, at a measuring AC voltage of 50 mV and different bias voltages between 0 V and 4 V. Measurements were carried out with a computer-controlled impedance analyzer Hewlett-Packard 4192A combined with a Novotherm temperature control system (Novocontrol).

3 Results and discussion

Raman spectra (fig. 1) of the employed multi-wall carbon nanotubes exhibit the characteristic bands in good agreement with existing literature. For a detailed interpretation of the obtained Raman spectra we used the results of refs. [32,33]. Three dominating peaks are observed: the *D* (disorder) band, the *G* (graphite) band and their second-order harmonic (the *G'* band). The *D* band of MWCNTs with a maximum at $1323\ \text{cm}^{-1}$ indicates the defects in the crystal structure, and impurities, including amorphous carbon. The *G* band (at $\sim 1590\ \text{cm}^{-1}$) has a doublet structure: G_1 ($1583\ \text{cm}^{-1}$) and G_2 ($1605\ \text{cm}^{-1}$), which originate from tangential vibrations parallel and perpendicular to the nanotube axis.

From tapping mode AFM images (fig. 2), the length distribution of the multi-wall nanotubes was determined from 70 individual measurements before sonification. Figure 3 depicts the obtained histogram of the length distribution of the dispersed MWCNTs. The distribution function has a maximum at approximately 900 nm, corresponding to the average length of the nanotubes. The

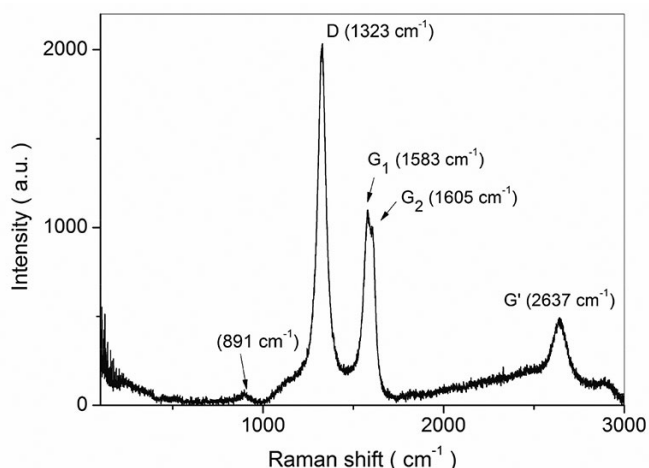


Fig. 1. Raman spectrum of a bundle of multi-wall carbon nanotubes. The characteristic D , G , and G' bands are observed at wave numbers in agreement with existing literature.

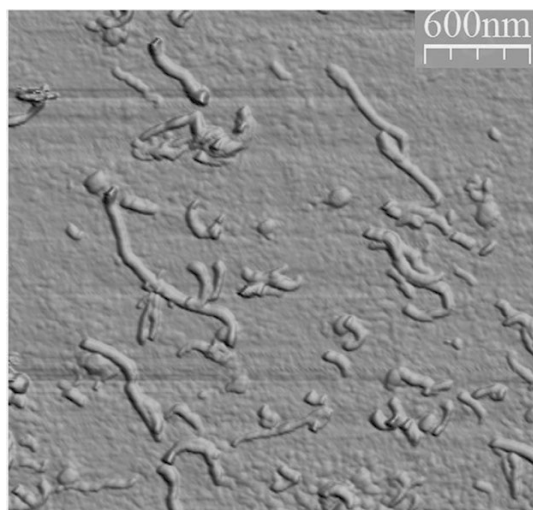


Fig. 2. Exemplary AFM image of dispersed multi-wall carbon nanotubes on a glass surface.

length distribution appears to have a short length cut off, which is possibly due to measurement technique. Nevertheless, the important parameter is the average nanotube length, which can clearly be determined. The nanotube width is quite thick, which is most likely also related to the measurement technique, while defects can clearly be observed showing that the nanotubes are not straight.

Optical polarizing investigations have shown that the textures of pure as well as doped materials were identical. This implies that the nanotubes did not disturb the molecular orientation of the liquid crystal at a scale of optical wavelengths or larger. The phase diagram of the FLC-MWCNT mixtures is shown in fig. 4. Doping of carbon nanotubes into the FLC leads to a small decrease of the clearing point, and a more pronounced depression of other phase transition temperatures. The temperature range of the SmA^* phase essentially widens by about 10 K with increasing nanotube concentration. The shift of the

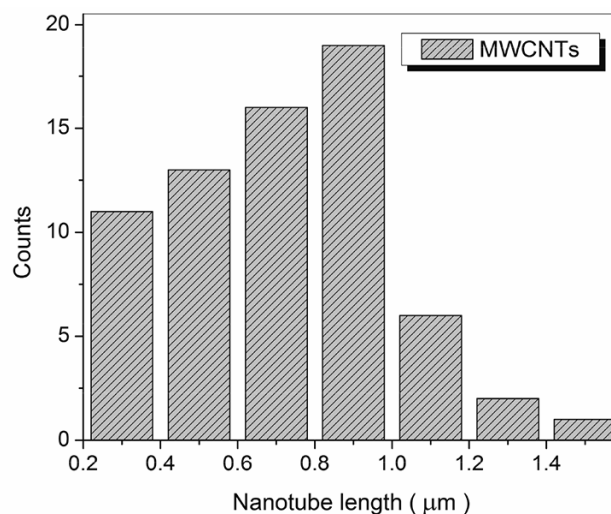


Fig. 3. Length distribution of the dispersed MWCNTs as determined by atomic force microscopy. The material is relatively polydisperse with an average length of the nanotubes of approximately 900 nm.

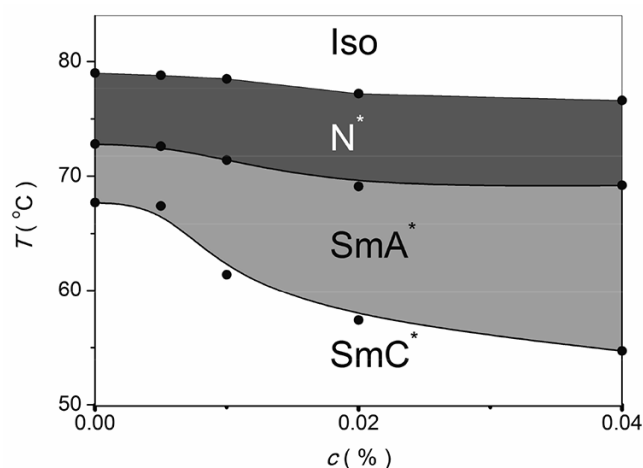


Fig. 4. Phase diagram of the FLC-MWCNTs mixtures determined by polarizing microscopy.

SmC^* - SmA^* transition temperature, T_c , is accounted for by presenting all data below as a function of reduced temperature $T - T_c$. The decrease of the paraelectric to ferroelectric transition temperature (SmA^* to SmC^*) is quite substantial. This can be followed by several different techniques, polarizing microscopy for the clearing point and the nematic to SmA^* transition, and electrical measurements for the SmA^* - SmC^* transition, which is harder to detect by microscopy.

Measurements of the temperature dependence of the SmC^* tilt angle θ (fig. 5) show a substantial decrease with increasing dopant concentration. Such behavior has also been reported by other groups [29]. The inset of fig. 5 shows that the tilt angle decreases approximately linearly with increasing nanotube concentration.

One of the most important properties of FLCs is the spontaneous polarization P_S , which appears in chiral

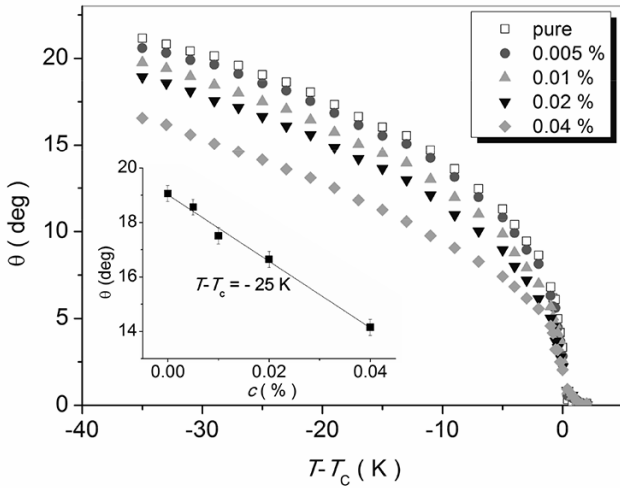


Fig. 5. Temperature dependence of the tilt angle of the FLC-MWCNT dispersions. The tilt angle decreases linearly with increasing nanotube concentration as shown in the inset for a reduced temperature of $T - T_c = -25$ K.

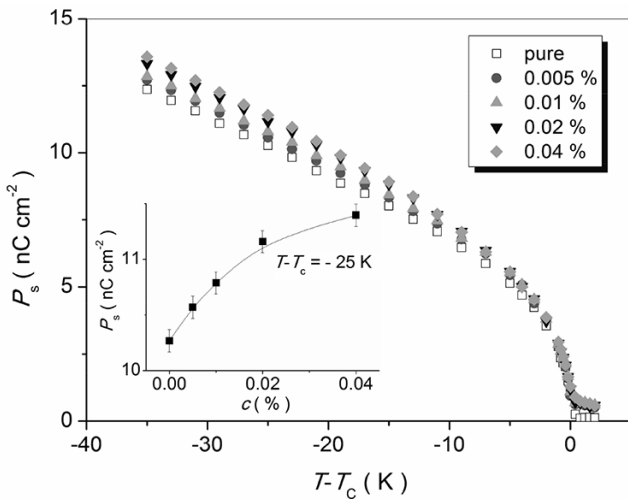


Fig. 6. Temperature dependence of the spontaneous polarization of FLC-MWCNT dispersions for several nanotube concentrations. The concentration behavior of the spontaneous polarization is shown in the inset for a reduced temperature of $T - T_c = -25$ K.

tilted smectic mesophases due to the long-range ordering of molecular transverse dipoles and depends on the transverse component μ_t of the molecular dipole. The temperature and concentration dependence of the spontaneous polarization at applied electric field amplitude of $1.07 \text{ V}/\mu\text{m}$ and frequency 70 Hz are shown in fig. 6. The introduction of MWCNTs increases P_S in comparison with the neat FLC material. It is anticipated that such behavior may be due to the interaction between the molecular dipole moment of the FLC and the induced dipole moment of the MWCNTs, enhancing the spontaneous polarization. The spontaneous polarization at a fixed reduced temperature of $T - T_c = -25 \text{ K}$ exhibits an increase with increasing nanotube concentration, until saturation is observed at

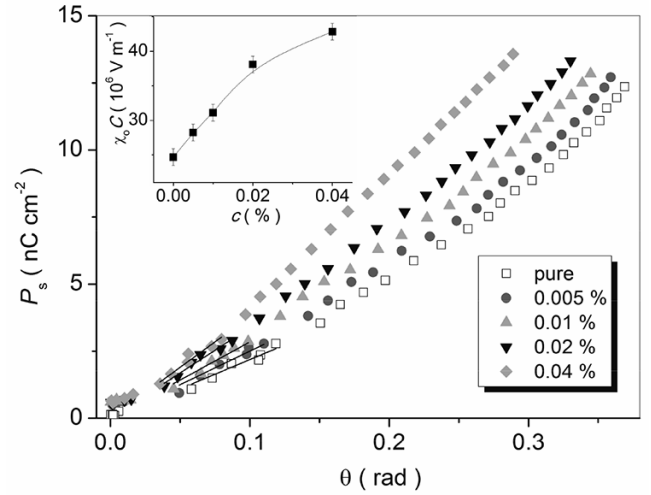


Fig. 7. The initial slope of the experimental polarization *versus* tilt data can be used to determine the quantity $\chi_0 C$, which is related to the bilinear polarization-tilt coupling of the FLC-MWCNT dispersions. The inset indicates that for small nanotube concentrations this coupling increases linearly with concentration.

concentrations of approximately $c > 0.04 \text{ wt}\%$ (inset of fig. 6).

In the classic Landau theory of FLCs [34–36], the magnitude of the spontaneous polarization in first approximation depends linearly on the tilt angle (eq. (1)),

$$P_S \approx \varepsilon_0 \chi_0 C \theta, \quad (1)$$

where ε_0 is the vacuum permittivity, χ_0 is the dielectric susceptibility and C is the bilinear polarization-tilt coupling coefficient. From the initial slope $dP_S/d\theta$ of the $P_S(\theta)$ plots (fig. 7) the quantity $\chi_0 C$, which relates to the bilinear polarization-tilt coupling, can be determined as a function of nanotube concentration. The inset of fig. 7 demonstrates that the coupling increases practically linearly with increasing dopant concentration, at least for small concentrations.

In consideration of the important role of the electro-optical switching time and the viscosity of ferroelectric liquid crystals for the operation of devices, we investigated the effect of multi-wall carbon nanotubes on the performance of FLCs. Figure 8 depicts the temperature dependence of the rise time, normally defined as the change in transmission from 10% to 90%. As expected, the response time decreases with increasing temperature, due to the temperature dependence of the material viscosity. In addition, the response time increases with increasing nanotube concentration, as shown in the inset of fig. 8. This behavior may be explained by the strong LC-MWCNT anchoring interaction as well as the large size of carbon nanotubes as compared to the size of a mesogen. The addition of nanotubes to the neat FLC increases the rotational viscosity, and thus the electro-optic response times. This result is in contrast to previous reports [23, 24, 29]. There, it is argued that the induced polarization of the nanotubes screens the spontaneous polarization, thus reducing it as compared to

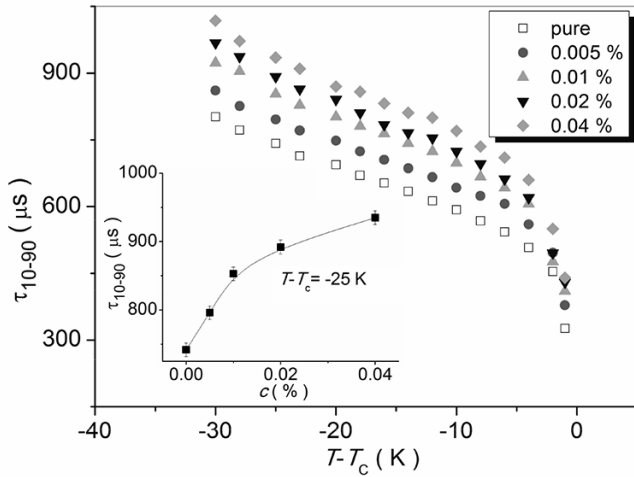


Fig. 8. Temperature dependence of the rise time for several FLC-MWCNT dispersions at different concentrations. The concentration dependence of the rise time τ_{10-90} at a reduced temperature of $T - T_c = -25$ K is shown in the inset.

the neat FLC. According to eq. (2)

$$\tau = \frac{\gamma}{P_S E} \quad (2)$$

this would on the other hand imply an increase in response time, opposite to what was observed. In our case we observe an increase in spontaneous polarization with increasing nanotube concentration (fig. 6), as well as an increase of response times (fig. 8). This behavior can thus not be attributed to effects of polarization, but rather to an increase in rotational viscosity with increasing nanotube concentration (see inset of fig. 8).

Rewriting eq. (2), the rotational viscosity γ_1 was calculated from polarization and switching time measurements, according to eq. (3)

$$\gamma_1 = \tau P_S E. \quad (3)$$

The respective temperature and nanotube concentration dependence is depicted in fig. 9. We deliberately plotted this as a function of reduced temperature, because the dependence on nanotube concentration is then better revealed. Obviously, the large increase in rotational viscosity is due to the decrease in absolute temperature. The further increase is then caused by the additional effect of the nanotubes and their increasing concentration. In general, addition of MWCNTs to the ferroelectric liquid crystal causes an increase in rotational viscosity, and thus accounts for the slower response times discussed above. It is anticipated that the change of electrooptic parameters is related to the interaction between the liquid crystal molecules and the graphitic surface of the carbon nanotubes.

At last, we carried out dielectric spectroscopic investigations of the respective dispersions, especially with respect to the Goldstone-mode, *i.e.* director fluctuations on the tilt cone. Measurements were performed in the frequency range of 5 Hz–13 MHz, but only data up to 10^4 Hz

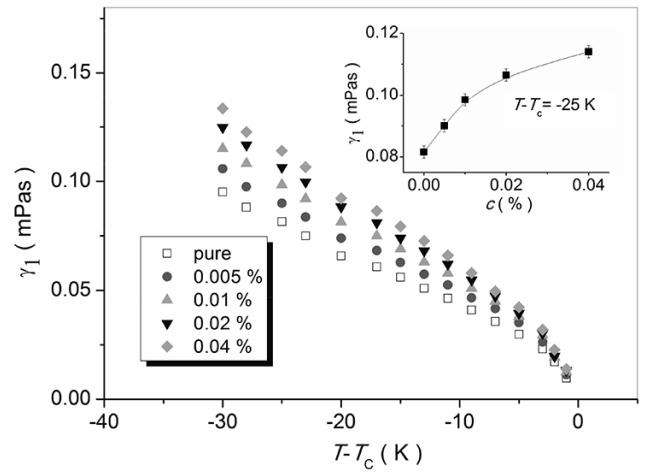


Fig. 9. Temperature dependence of the rotational viscosity of FLC-MWCNT dispersions. The concentration behavior of the rotational viscosity of the investigation mixtures at a reduced temperature of $T - T_c = -25$ K is shown in the inset.

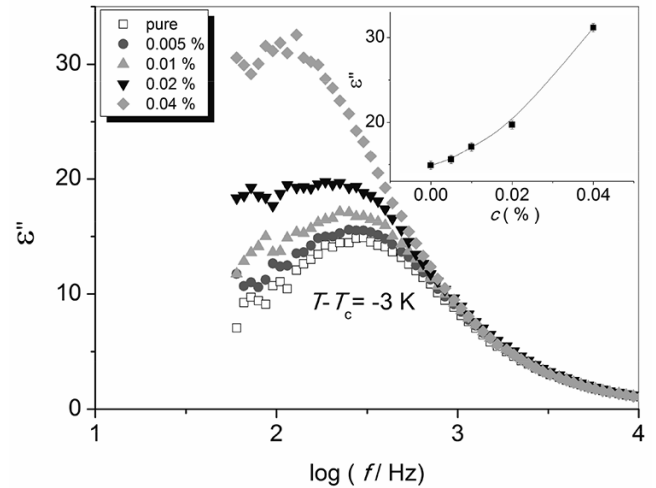


Fig. 10. Frequency dependence of the imaginary part of the dielectric permittivity of the FLC-MWCNT dispersions at a reduced temperature of $T - T_c = -3$ K and applied AC measuring voltage of 50 mV (without bias). The concentration dependence is summarized in the inset.

will be displayed, because for frequencies $f > 10^5$ Hz the so called ITO-mode falsifies the actual spectra of the material alone. Figure 10 depicts the imaginary part of the dielectric permittivity ϵ'' as a function of frequency of the FLC-MWCNT dispersions at a reduced temperature of $T - T_c = -3$ K without a bias voltage applied. Doping of carbon nanotubes in FLCs thus leads to an increase of the maximum value of ϵ'' with increasing dopant concentration. This behavior is consistent with observations by Gupta *et al.* [28] and Shukla *et al.* [26], opposed to reports by Podgornov *et al.* [23], Arora *et al.* [25], and Malik *et al.* [29]. Nevertheless, the observed increase in spontaneous polarization (fig. 6) would rather favor the behavior depicted in fig. 10, as the Goldstone-mode dielectric strength is strongly dependent on polarization and tilt angle with

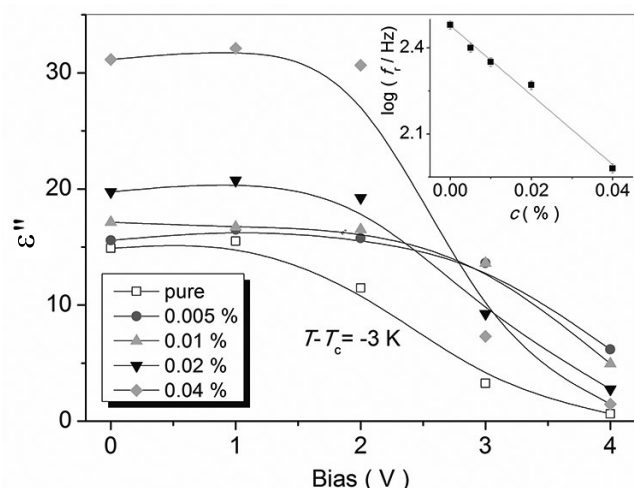


Fig. 11. Dependence of the imaginary part of the dielectric permittivity of the FLC-MWCNT dispersions on bias voltage (lines are a guide to the eye). The dependence of the Goldstone-mode relaxation frequency on nanotube concentration is shown in the inset.

$\Delta\epsilon \sim (P_S/\theta)^2$, a quantity which increases with increasing nanotube concentration (fig. 7).

Moreover, the relaxation frequency, f_r , of the Goldstone mode shifts towards the low-frequency region for increasing nanotube concentration (fig. 11). This decrease of relaxation frequency is practically linearly dependent on concentration, as shown in the inset of fig. 11, and is qualitatively consistent with reports in the literature [25, 28]. It can be understood in terms of the increasing viscosity, as Goldstone-mode relaxation frequency and viscosity are inversely proportional, *i.e.* $f_r \sim 1/\gamma$.

4 Conclusions

We presented a detailed account of the main physical properties of ferroelectric liquid crystal-carbon nanotube dispersions, namely tilt angle, spontaneous polarization, bilinear polarization-tilt coupling, response time, rotational viscosity, and dielectric Goldstone-mode relaxation strength and frequency. Despite a clearly decreasing tilt angle, the spontaneous polarization increases as a function of nanotube concentration. This was attributed to a possible dipole moment due to the presence of the nanotubes, and also accounts for the increase in the bilinear coupling coefficient and the dielectric relaxation strength. Even though the spontaneous polarization increases, the electro-optic response times of the mixtures nevertheless become slower for increasing nanotube concentration, which can only be explained by an increase in rotational viscosity. The latter in first approximation also explains the observed decrease in Goldstone-mode relaxation frequency for increasing nanotube concentration, assuming that the elastic interactions of the liquid crystal host are not significantly altered.

M.Y. acknowledges the financial support of the DAAD through a Forschungskurzstipendium under grant number A/10/73108. Andreas Bogner is gratefully acknowledged for his help with the dielectric measurements. The authors would also like to thank Alberto Sánchez Castillo and Tobias Kittel for help with the Raman and AFM experiments, respectively.

References

1. R. Saito, G. Dresselhaus, M.S. Dresselhaus, *Physical Properties of Carbon Nanotubes* (Imperial College Press, London, 2001).
2. P.J. Collings, M. Hird, *Introduction to Liquid Crystals: Chemistry and Physics* (Taylor & Francis, London, 1997).
3. S. Chandrasekhar, *Liquid Crystals*, 2nd ed. (Cambridge University Press, Cambridge, 1992).
4. B. Meyer, L. Liebert, L. Strzelecki, P. Keller, *J. Phys. (Paris) Lett.* **36**, L69 (1975).
5. S.T. Lagerwall, *Ferroelectric and Antiferroelectric Liquid Crystals* (Wiley-VCH, Weinheim, 1999).
6. N.A. Clark, S.T. Lagerwall, *Appl. Phys. Lett.* **36**, 899 (1980).
7. M. Lynch, D. Patrick, *Nano Lett.* **2**, 1197 (2002).
8. I. Dierking, G. Scalia, P. Morales, D. Leclere, *Adv. Mater.* **16**, 865 (2003).
9. S. Kumar, H.K. Bisoyi, *Angew. Chem. Int. Ed.* **46**, 1501 (2007).
10. H.K. Bisoyi, S. Kumar, *J. Mater. Chem.* **18**, 3032 (2008).
11. H.K. Bisoyi, S. Kumar, *J. Ind. Inst. Sci.* **89**, 101 (2009).
12. J.P.F. Lagerwall, G. Scalia, M. Haluska, U. Dettlaff-Weglikowska, F. Giesselmann, S. Roth, *Phys. Status. Solidi B* **243**, 3046 (2006).
13. J. Lagerwall, G. Scalia, M. Haluska, U. Dettlaff-Weglikowska, S. Roth, F. Giesselmann, *Adv. Mater.* **19**, 359 (2007).
14. W. Jiang, B. Yu, W. Liu, J. Hao, *Langmuir* **23**, 8549 (2007).
15. G. Scalia, C. von Bühler, C. Hägele, S. Roth, F. Giesselmann, J.P.F. Lagerwall, *Soft Matter* **4**, 570 (2008).
16. V. Weiss, R. Thiruvengadathan, O. Regev, *Langmuir* **22**, 854 (2006).
17. S. Badaire, C. Zakri, M. Maugey, A. Derré, J.N. Barisci, G. Wallace, P. Poulin, *Adv. Mater.* **13**, 1673 (2005).
18. W. Song, A.H. Windle, *Macromolecules* **38**, 6181 (2005).
19. J.P.F. Lagerwall, G. Scalia, *J. Mater. Chem.* **18**, 2890 (2008).
20. I. Dierking, G. Scalia, P. Morales, *J. Appl. Phys.* **97**, 044309 (2005).
21. I. Dierking, K. Casson, R. Hampson, *Jpn. J. Appl. Phys.* **47**, 6390 (2008).
22. I. Dierking, S.E. San, *Appl. Phys. Lett.* **87**, 233507 (2005).
23. F.V. Podgornov, A.M. Suvorova, A.V. Lapanik, W. Haase, *Chem. Phys. Lett.* **479**, 206 (2009).
24. J. Prakash, A. Chaudhary, D.S. Mehta, A.M. Biradar, *Phys. Rev. E* **80**, 012701 (2009).
25. P. Arora, A. Mikulko, F. Podgornov, W. Haase, *Mol. Cryst. Liq. Cryst.* **502**, 1 (2009).
26. R.K. Shukla, K.K. Raina, V. Hamplová, M. Kašpar, A. Bubnov, *Phase Trans.* **84**, 850 (2011).

27. S. Ghosh, P. Nayek, S.K. Roy, R. Gangopadhyay, M.R. Molla, T.P. Majumder, Eur. Phys. J. E **34**, 35 (2011).
28. S.K. Gupta, A. Kumar, A.K. Srivistava, R. Manohar, J. Non-Cryst. Solids **357**, 1822 (2011).
29. P. Malik, A. Chaudhary, R. Mehra, K.K. Raina, J. Mol. Liq. **165**, 7 (2012).
30. V.N. Vijayakumar, M.L.N.M. Mohan, J. Disp. Sci. Tech. **33**, 111 (2012).
31. K. Miyasato, S. Abe, H. Takezoe, A. Fukuda, E. Kuze, Jpn. J. Appl. Phys. **22**, L661 (1983).
32. A.M. Rao, E. Ritcher, S. Bandow, B. Chase, P.C. Eklund, K.A. Williams, S. Fang, K.R. Subbaswamy, M. Menon, A. Thess, R.E. Smalley, G. Dresselhaus, M.S. Dresselhaus, Science **275**, 187 (1997).
33. M.S. Dresselhaus, G. Dresselhaus, A. Jorio, A.G. Souza Filho, R. Saito, Carbon **40**, 2043 (2002).
34. B. Žekš, Mol. Cryst. Liq. Cryst. **114**, 259 (1984).
35. T. Carlsson, B. Žekš, A. Levstik, C. Filipic, I. Levstik, R. Blinc, Phys. Rev. A **36**, 1484 (1987).
36. F. Giesselmann, A. Heimann, P. Zugenmaier, Ferroelectrics **200**, 237 (1997).